CMS Physics Analysis Summary

Contact: cms-pag-conveners-susy@cern.ch 2021/07/26

Search for direct pair production of supersymmetric partners to the τ lepton in the all-hadronic final state at $\sqrt{s} = 13$ TeV

The CMS Collaboration

Abstract

A search for the direct production of a pair of τ sleptons in proton-proton collisions at a center-of-mass energy of 13 TeV is presented. The search is carried out in events with two τ leptons, each decaying to one or more hadrons and a neutrino. In addition to scenarios in which the τ sleptons decay promptly, the search also addresses scenarios in which the τ sleptons have macroscopic lifetimes, giving rise to displaced τ leptons. The data were collected with the CMS detector from 2016 to 2018, and correspond to an integrated luminosity of 137 fb^{-1}. No significant excess is seen in the observed event counts with respect to the standard model background expectation. Limits on pair production of both promptly decaying and long-lived τ sleptons are obtained in the framework of simplified models in which the τ slepton decays to a τ lepton and the lightest supersymmetric particle (LSP), which is assumed to be stable. In the case of purely left-handed τ slepton pair production, with a prompt decay to a τ lepton and a nearly massless LSP, τ slepton masses between 115 and 340 GeV are excluded. In a scenario with macroscopic τ slepton decay lengths corresponding to $c\tau_0 = 0.1$ mm, τ slepton masses between 150 and 220 GeV are excluded for the case that the LSP is nearly massless.

1 Introduction

Supersymmetry (SUSY) [1–8] is appealing because it could help to address some of the shortcomings of the standard model (SM) of particle physics. It features the presence of superpartners for SM particles with the same quantum numbers other than the spin, which is different by half a unit. The contributions of the superpartners, which could help to cancel the quadratic divergences in radiative corrections to the Higgs boson mass from SM particles, could resolve the fine tuning problem [9–12]. In SUSY models with R-parity conservation [13], the lightest supersymmetric particle (LSP) is stable and could be a dark matter (DM) candidate [14–16].

In this note, we report the results of a search targeting the τ slepton ($\widetilde{\tau}$), the superpartner of the τ lepton. Early universe $\widetilde{\tau}$-neutralino coannihilation models provide a mechanism that can explain the observed DM relic density [17–22]. They motivate the existence of a light $\widetilde{\tau}$ as the next-to-lightest supersymmetric particle (NLSP), which would lead to an enhanced rate of production of final states with τ leptons in collider experiments [23, 24]. Here, we study events with two τ leptons, both undergoing hadronic decays (τ_{h}), and with significant transverse momentum imbalance. While previous searches in this final state have largely focused on prompt decays of the parent particles, this search also addresses scenarios in which the $\widetilde{\tau}$ is long-lived, giving rise to displaced τ_{h}. Such scenarios can arise easily in theories of gauge-mediated SUSY breaking (GMSB), which frequently predict a $\widetilde{\tau}$ as the NLSP [25].

Figure 1 shows the simplified model [26–28] of direct $\widetilde{\tau}$ pair production, with the $\widetilde{\tau}$ decaying to a τ lepton and the LSP, which we study in this note. For models featuring prompt decays of the $\widetilde{\tau}$, we assume $\widetilde{\chi}_1^0$, the lightest neutralino, to be the LSP, and consider a range of $\widetilde{\chi}_1^0$ masses up to 200 GeV. We explore models in which the $\widetilde{\tau}$ can be either the $\widetilde{\tau}_{\mathrm{L}}$ or $\widetilde{\tau}_{\mathrm{R}}$, the superpartners of left- or right-handed τ leptons, respectively, and study cases in which only $\widetilde{\tau}_{\mathrm{L}}$ or only $\widetilde{\tau}_{\mathrm{R}}$ pairs are produced, as well as a degenerate case in which both $\widetilde{\tau}_{\mathrm{L}}$ and $\widetilde{\tau}_{\mathrm{R}}$ pairs are produced. The small production cross section expected for the signal, and significant SM backgrounds, make this search challenging. Previous searches for direct $\widetilde{\tau}$ pair production in prompt decay scenarios were performed at the CERN LEP collider [29–32], and excluded $\widetilde{\tau}$ masses at 95% confidence level (CL) up to $\approx$90 GeV for neutralino masses up to 80 GeV in some models. The ATLAS [33, 34] and CMS [35] Collaborations performed searches for direct $\widetilde{\tau}$ pair production using 8 TeV LHC data. The ATLAS Collaboration has reported the results of a search for direct $\widetilde{\tau}$ pair production using 13 TeV data corresponding to an integrated luminosity of 139 fb^{-1} [36], while the CMS Collaboration has previously reported the results of a search for direct $\widetilde{\tau}$ pair production using 77.2 fb^{-1} of data collected in 2016 and 2017 at 13 TeV [37].

We also target scenarios where the $\widetilde{\tau}$ has a macroscopic lifetime, decaying within a few cm of the primary interaction and producing signatures with displaced τ_{h}. These signatures are sensitive to GMSB SUSY models in which a nearly massless gravitino is the LSP, and the $\widetilde{\tau}$ is the NLSP that can become long-lived as a result of its small decay width. We consider models involving the pair production of $\widetilde{\tau}_1$, a mixture of $\widetilde{\tau}_{\mathrm{L}}$ and $\widetilde{\tau}_{\mathrm{R}}$, in which the $\widetilde{\tau}_1$ decays to a τ lepton and a nearly massless LSP, for mean proper decay lengths, $c\tau_0$, up to 2.5 mm. For these models, we assume a scenario with maximal mixing, i.e. with a mixing angle of $\frac{\pi}{4}$, for which the cross section is very similar to that for purely right-handed $\widetilde{\tau}$ pair production [38]. This scenario is therefore consistent with GMSB SUSY models, in which the $\widetilde{\tau}$ is typically right-handed. Previously, the LEP experiments set limits on GMSB SUSY models with $\widetilde{\tau}_1$ as the NLSP, with the strongest limits coming from the OPAL experiment [39]. The OPAL limits excluded masses up to 87.4 GeV at 95% CL, for all $\widetilde{\tau}_1$ lifetimes. The ATLAS Collaboration recently reported the results of a search for long-lived sleptons, including $\widetilde{\tau}_{1,2}$, a combination of mixed states of $\widetilde{\tau}_{\mathrm{L}}$ and $\widetilde{\tau}_{\mathrm{R}}$ with the degenerate production of the two mixed states $\widetilde{\tau}_1$ and $\widetilde{\tau}_2$, in final states with

displaced electrons and muons. The search excluded $\widetilde{\tau}_{1,2}$ masses up to 340 GeV for a proper lifetime of 0.1 ns [40].

This note presents an update of the search reported in Ref. [37], for final states with two τ_{h}. The data collected with the CMS detector in 2018 has been incorporated, resulting in a sample corresponding to a total integrated luminosity of 137 fb^{-1} and a significant improvement in the search sensitivity. Improved techniques are used to describe the SM background with τ leptons through a method called "embedding," [41] which estimates the background with two genuine τ_{h} from data, with minimal input from simulation. As noted above, this analysis also targets scenarios in which the $\widetilde{\tau}$ is long-lived.

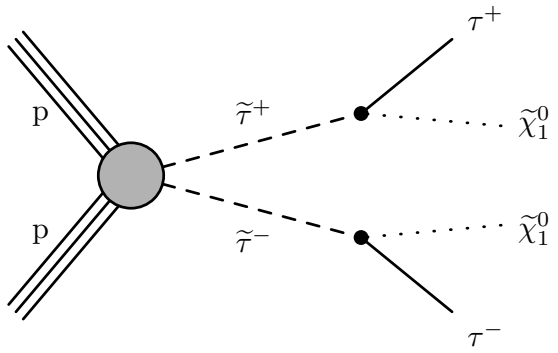

Figure 1: Diagram for direct $\widetilde{\tau}$ pair production, followed by decay of each $\widetilde{\tau}$ to a τ lepton and a $\widetilde{\chi}_1^0$.

2 The CMS detector

The central feature of the CMS apparatus is a superconducting solenoid of 6 m internal diameter, providing a magnetic field of 3.8 T. A silicon pixel and strip tracker, a lead tungstate crystal electromagnetic calorimeter (ECAL), and a brass and scintillator hadron calorimeter, each composed of a barrel and two endcap sections, reside within the solenoid volume. Forward calorimeters extend the pseudorapidity (η) coverage provided by the barrel and endcap detectors. Muons are detected in gas-ionization chambers embedded in the steel flux-return yoke outside the solenoid. Events of interest are selected using a two-tiered trigger system [42]. The first level, composed of custom hardware processors, uses information from the calorimeters and muon detectors to select events at a rate of around 100 kHz within a time interval of less than 4 μs. The second level, known as the high-level trigger, consists of a farm of processors running a version of the full event reconstruction software optimized for fast processing, which reduces the event rate to about 1 kHz before data storage. A more detailed description of the CMS detector, together with definitions of the coordinate system and kinematic variables, can be found in Ref. [43].

3 Event reconstruction and simulation

The event reconstruction uses a particle-flow (PF) algorithm [44], which aims to reconstruct and identify each individual particle in an event, with an optimized combination of information from the various elements of the CMS detector. The missing transverse momentum vector, $\vec{p}_{\mathrm{T}}^{\,\mathrm{miss}}$, is computed as the negative of the vector sum of the transverse momentum (p_{T}) of all PF

candidates reconstructed in an event. Its magnitude, $p_{\mathrm{T}}^{\mathrm{miss}}$ [45], is used in the search as a discriminator between signal and SM background. Events selected for the search are required to pass selection criteria [45] designed to remove anomalous high-$p_{\mathrm{T}}^{\mathrm{miss}}$ events that can occur due to a variety of reconstruction failures, detector malfunctions or non collisions backgrounds, and must have at least one reconstructed interaction vertex. Additional proton-proton interactions within the same or nearby bunch crossings (pileup) can lead to the reconstruction of multiple vertices in a proton-proton (pp) collision event. The reconstructed vertex with the largest value of summed object p_{T}^2 is selected to be the primary pp interaction vertex (PV). These objects are the jets, clustered using a jet finding algorithm [46, 47] with the tracks assigned to a given vertex as inputs, and the associated missing transverse momentum, taken as the negative vector sum of the p_{T} of those jets.

Charged particles that originate from the PV, photons, and neutral hadrons are clustered into jets using the anti-k_{T} algorithm [46, 47] with a distance parameter of 0.4. The jet energies are corrected to account for the contribution from pileup interactions and to compensate for variations in the detector response [47, 48]. The jets considered in this analysis are required to be within the tracker volume, $|\eta| < 2.4$, and to satisfy the condition $p_{\mathrm{T}} > 30\,\mathrm{GeV}$. They are required to be separated in the plane of η and azimuthal angle (ϕ) by $\Delta R \equiv \sqrt{(\Delta\eta)^2 + (\Delta\phi)^2} > 0.4$ from τ_{h} candidates in order to avoid the double counting of objects. The deep neural network (DNN) based combined secondary vertex algorithm (DeepCSV) [49] is used to identify, or 'tag', jets originating from the hadronization of b quarks in order to reject events with b quark jets that are likely to originate from SM backgrounds with top quarks. A high-efficiency ("Loose") working point is used, with an efficiency of ≈84% for tagging b quarks originating from top quark decays, and misidentification rates of about 41 and 11%, respectively, for jets from charm quarks, and from light quarks or gluons.

In order to suppress SM backgrounds such as those originating from diboson production or $\mathrm{t\bar{t}}$ production in association with a vector boson, we veto events with electron or muon candidates. We identify these using the same selection criteria as those described in Ref. [37]. The τ_{h} candidates are reconstructed from jets, using the hadrons-plus-strips algorithm [50], which combines 1 or 3 tracks with energy deposits in the calorimeters, to identify the hadronic τ lepton decay modes. Decay modes with one or three charged hadrons, and with or without neutral pions, are considered in this search. To distinguish genuine τ_{h} decays from jets originating from the hadronization of quarks or gluons, and from electrons or muons, a multi-class DNN-based algorithm, the CMS "DeepTau" algorithm is used. Information from all individual reconstructed particles near the τ_{h} axis is combined with properties of the τ_{h} candidate and event activity. We employ two working points of the anti-jet DeepTau discriminant: a relaxed ("Loose"), and a more stringent ("VVTight") working point. These working points correspond to efficiencies of ≈80 and ≈40%, respectively, for a genuine τ_{h}, and misidentification rates of ≈0.5 and ≈0.06%, respectively, for quark or gluon jets.

Monte Carlo (MC) simulation is used to model the signal. The MADGRAPH5_aMC@NLO version 2.3.3 and 2.4.2 event generators [51] are used at leading order (LO) precision to generate models of direct $\widetilde{\tau}$ pair production for promptly decaying $\widetilde{\tau}$ up to the production of τ leptons, with their decay modeled by PYTHIA 8.212 or 8.230 [52], depending on the data-taking year. For signal models in which the $\widetilde{\tau}$ has a macroscopic decay length, the $\widetilde{\tau}$ pair production process is generated with MADGRAPH5_aMC@NLO at LO precision, with the $\widetilde{\tau}$ decays being subsequently carried out by PYTHIA. The CUETP8M1 underlying-event tune [53] is used with PYTHIA for simulation samples corresponding to the 2016 data set, and the CP5 tune [54] is used for 2017 and 2018 samples. The NNPDF3.0LO [55] set of PDFs is used in generating the 2016 simulation samples, while the NNPDF3.1 next-to-leading order (NLO) PDFs are used for

2017 and 2018. Showering and hadronization of partons are carried out using PYTHIA, while a detailed simulation of the CMS detector is based on the GEANT4 [56] package. Finally, uncertainties in renormalization and factorization scale have been obtained using the SYSCALC package [57].

We also use MC simulation to model the background from SM Higgs bosons. The POWHEGv2 [58–61] generator is used to produce samples of Higgs boson events with decays to τ pairs. Other backgrounds, originating from processes that give rise to two genuine τ_h, or to one or more jets that are misidentified as τ_h, are estimated from data, as described in Section 5. The background from events in which an electron or muon is misidentified as a τ_h is negligible.

Simulated events are reweighted to match the pileup profile observed in data. Scale factors are applied to numbers obtained from the simulation in order to account for differences in trigger efficiencies, τ_h identification efficiencies, jet and τ_h energy scales, and b tagging efficiency with respect to data. We improve the modeling of initial-state radiation (ISR) in the 2016 signal simulation samples by reweighting the p_T^{ISR} distribution, where p_T^{ISR} corresponds to the total transverse momentum of the system of SUSY particles. This reweighting procedure is based on studies of the p_T of Z bosons [62]. No corrections were found to be necessary for the p_T^{ISR} distribution in 2017 and 2018 simulation samples, as the ISR modeling was improved in the simulation. The signal production cross sections are calculated at next-to-leading order (NLO) using next-to-leading logarithmic (NLL) soft-gluon resummations [38].

Since the embedded samples used to model the genuine τ_h background rely on data for the description of the underlying event and additional jet production, no corrections for the pileup profile, jet energy scale, or b tagging efficiency are needed for these samples. Correction factors are applied to account for the efficiencies of the dimuon triggers and muon identification and isolation criteria used to select events for embedding. As the τ lepton decays are simulated with PYTHIA, we apply scale factors in order to match the τ_h identification efficiency and energy scale in data. Correction factors are also applied to match the efficiencies of triggers used to select events for the search in data. Since the tracking efficiency in embedded events is higher than in data, scale factors are applied to account for this discrepancy. In order to save computing time by restricting the sample selected for detector simulation to events that will subsequently satisfy the selection criteria applied in analyses, a kinematic filtering is imposed on the p_T and $|\eta|$ of the visible τ lepton decay products prior to carrying out the detector simulation. Event weights are applied in order to account for the bias arising from the filter requirements. These corrections are described in more detail in Ref. [41].

4 Event selection

The search strategy relies on a simultaneous maximum likelihood fit of the event yields observed in 31 search regions (SRs), which are described below. The data used in this search are selected with two sets of triggers. For events with $p_T^{miss} < 200\,GeV$, we use a trigger requiring the presence of two τ_h candidates, each with $p_T > 35$ (>40) GeV in 2016 (2017 and 2018) data. We gain signal efficiency for events with $p_T^{miss} > 200\,GeV$ by using a p_T^{miss}-based trigger, with a threshold varying between 100 and 140 GeV, depending on the data-taking period.

Following the trigger selection, we impose a baseline event selection requiring the presence of exactly two τ_h candidates of opposite charge with $p_T > 40\,GeV$, $|\eta| < 2.1$, and satisfying the "VVTight" DeepTau selection and other criteria described in Section 3. Backgrounds originating from diboson production or $t\bar{t}$ production in association with a vector boson are suppressed by vetoing events with electron or muon candidates with $p_T > 20\,GeV$ and $|\eta| < 2.5$ or <2.4

for electrons and muons respectively, or additional τ_h candidates with $p_T > 30\,\text{GeV}$ satisfying the "Loose" DeepTau selection. We reject any events with a b-tagged jet to suppress top quark backgrounds, and require $|\Delta\phi(\tau_h^{(1)}, \tau_h^{(2)})| > 1.5$ to reduce the background from $Z/\gamma* \to \tau\tau$ events, while retaining high signal efficiency. Finally, we require $p_T^{\text{miss}} > 50\,\text{GeV}$ to suppress the background with two misidentified τ_h. In order to avoid effects related to jet mismeasurement that can contribute to spurious p_T^{miss}, we require the $\vec{p}_T^{\text{miss}}$ to have a minimum separation of 0.25 in $|\Delta\phi|$ from reconstructed jets.

We use a number of discriminants to subdivide events satisfying the baseline selection criteria into exclusive SRs. For signal events, we expect the two stable LSPs in the final state to contribute to the p_T^{miss}. Consequently, we expect the correlations between $\vec{p}_T^{\text{miss}}$ and the reconstructed τ_h candidates to be different between signal and background events. Mass observables calculated from the τ_h transverse momenta and $\vec{p}_T^{\text{miss}}$ can be used to exploit these differences and discriminate signal from background.

One of the discriminants used is Σm_T, the sum of the transverse masses (m_T) calculated for each τ_h with p_T^{miss}, given by

$$\Sigma m_T = m_T(\tau_h^{(1)}, \vec{p}_T^{\text{miss}}) + m_T(\tau_h^{(2)}, \vec{p}_T^{\text{miss}}), \tag{1}$$

where the transverse mass for each τ_h is defined as

$$m_T(\tau_h, \vec{p}_T^{\text{miss}}) \equiv \sqrt{2 p_T^{\tau_h} p_T^{\text{miss}} [1 - \cos\Delta\phi(\vec{p}_T^{\tau_h}, \vec{p}_T^{\text{miss}})]}. \tag{2}$$

For our signal models, p_T^{miss} can originate from neutrinos from τ lepton decays as well as from LSPs. However, the predominant contribution to the p_T^{miss} is expected to come from the LSPs, which we assume to be massless in the calculation of m_T.

We also use the "stransverse mass" m_{T2} [63–65], given by

$$m_{T2} = \min_{\vec{p}_T^{X(1)} + \vec{p}_T^{X(2)} = \vec{p}_T^{\text{miss}}} \left[\max\left(m_T^{(1)}, m_T^{(2)} \right) \right], \tag{3}$$

where $\vec{p}_T^{X(i)}$ (with i=1, 2) are the unknown transverse momenta of the two invisible particles, X(1) and X(2), corresponding to the LSPs in our signal models, and $m_T^{(i)}$ are the transverse masses obtained by assigning either of the two LSPs to one of the two parent $\tilde{\tau}$ decays. Once again, we assume the LSPs to be massless, and that the contribution from neutrinos from τ lepton decays to the p_T^{miss} will be negligible in comparison to the contribution from the LSPs. The minimization (min) is performed over the possible LSP momenta, which are constrained to add up to the $\vec{p}_T^{\text{miss}}$ in the event. For signal events, m_{T2} is expected to increase with the mass difference between the $\tilde{\tau}$ and LSP. We expect large values of m_{T2} to occur more frequently in signal events for models with larger $\tilde{\tau}$ masses, and to occur relatively rarely in SM background events.

Two sets of SRs are defined: the "prompt" SRs, targeting models in which the $\tilde{\tau}$ decays promptly, and the "displaced" SRs, targeting long-lived $\tilde{\tau}$ models.

An initial selection of $m_{T2} > 25\,\text{GeV}$ and $\Sigma m_T > 200\,\text{GeV}$ is required for all prompt SRs. In order to orthogonalize the prompt and displaced SRs, we require that events in the prompt SRs have at least one τ_h that does not satisfy the "displaced τ_h" criteria described below for the displaced SRs. Events are then subdivided into bins of m_{T2} and Σm_T, which provide sensitivity to a range of $\tilde{\tau}$ masses. We further subdivide events into two categories based on the

number of reconstructed jets (N_j): $N_j = 0$, and $N_j \geq 1$. Since background events that survive the SR kinematic selection criteria usually contain additional jets, the 0–jet category provides SRs with improved signal-to-background ratios. Signal events with ISR or pileup jets may populate the $N_j \geq 1$ SRs, and therefore we also retain these in order to avoid losing signal sensitivity. Finally, we gain additional sensitivity in bins with lower Σm_T and m_{T2} values in the 0–jet category, which have relatively high background, by further subdividing them into two bins based on the p_T of the leading (higher p_T) τ_h, $p_T^{\tau_h 1}$ ($p_T^{\tau_h 1} < 90\,\text{GeV}$, and $p_T^{\tau_h 1} \geq 90\,\text{GeV}$). This further improves signal vs background discrimination as the signal has higher τ_h p_T than the background.

The displaced category is defined by imposing the following "displaced τ_h" criteria for both τ_h candidates. We require the significance of the τ_h impact parameter relative to the PV in the transverse plane (d_{xy}), defined as the quantity divided by its uncertainty, to have an absolute value above 5, and the absolute value of its three-dimensional impact parameter (IP3D) to exceed 100 μm. We also require $m_{T2} > 25\,\text{GeV}, \Sigma m_T > 200\,\text{GeV}$, and $|\Delta\phi(\tau_h^{(1)}, \tau_h^{(2)})| > 1.75$ to further suppress the background in the displaced category. For events surviving these selection criteria, the p_T of the sub-leading (lower p_T) τ_h, $p_T^{\tau_h 2}$, provides additional discrimination between signal and the remaining background. Accordingly, we define two SR bins for events in this category, with $p_T^{\tau_h 2} < 110\,\text{GeV}$ and $p_T^{\tau_h 2} \geq 110\,\text{GeV}$, which were optimized to provide the best sensitivity.

Table 1 summarizes the Σm_T, m_{T2}, and $p_T^{\tau_h 1}$ criteria used to define the prompt SRs, and the $p_T^{\tau_h 2}$ criteria used to define the displaced SRs.

5 Background estimation

Significant contributions to the SM background to this search originate from $Z/\gamma* \to \tau\tau$, W+jets, $t\bar{t}$, and diboson processes, as well as from events exclusively comprising jets produced through the strong interaction of quantum chromodynamics (QCD), which we refer to as QCD multijet events. Smaller contributions arise from single top quark production and rare SM processes, such as triboson and Higgs boson production, and top quark pair production in association with vector bosons. We rely on a data-driven method to estimate the contributions of backgrounds in which one or both candidate τ_h are misidentified jets, consisting mainly of W+jets and QCD multijet events. We use a method known as "embedding" for modeling backgrounds with two genuine τ_h [41], by selecting dimuon events in data, removing the reconstructed muons, and embedding simulated τ leptons in their place. This method has the advantage that many event quantities are described by data and are not affected by imprecise modeling in simulation. The majority of the background with two genuine τ_h originates from $Z/\gamma* \to \tau\tau$ production, with smaller contributions originating from diboson production or processes with top quarks.

5.1 Estimation of background from misidentified jets

Events with misidentified τ_h candidates, originating predominantly from QCD multijet and W+jets production, constitute the dominant background after the requirement of two τ_h candidates with high p_T. We estimate this background using a data-driven method by extrapolating the event count in a data sample selected with a relaxed τ_h identification requirement, the Loose working point of the DeepTau discriminant, into the SR, following the same approach as that described in Ref. [37]. We measure the fraction of misidentified τ_h candidates selected with the Loose working point that also satisfy the VVTight requirement in a QCD multijet-enriched

Table 1: Ranges of Σm_{T}, m_{T2}, and $p_{\mathrm{T}}^{\tau_{\mathrm{h}}1}$ used to define the prompt search regions for the $N_{\mathrm{j}} = 0$ and $N_{\mathrm{j}} \geq 1$ event categories, and ranges of $p_{\mathrm{T}}^{\tau_{\mathrm{h}}2}$ used to define the displaced search regions.

Prompt SRs			
SR bin	Σm_{T} [GeV]	m_{T2} [GeV]	$p_{\mathrm{T}}^{\tau_{\mathrm{h}}1}$ [GeV]
$N_{\mathrm{j}} = 0$			
1	$200-250$	$25-50$	<90
2	$200-250$	$25-50$	>90
3	$200-250$	$50-75$	<90
4	$200-250$	$50-75$	>90
5	$200-250$	>75	—
6	$250-300$	$25-50$	<90
7	$250-300$	$25-50$	>90
8	$250-300$	$50-75$	<90
9	$250-300$	$50-75$	>90
10	$250-300$	>75	—
11	$300-350$	$25-50$	—
12	$300-350$	$50-75$	—
13	$300-350$	$75-100$	—
14	$300-350$	>100	—
15	>350	$25-50$	—
16	>350	$50-75$	—
17	>350	$75-100$	—
18	>350	>100	—
$N_{\mathrm{j}} \geq 1$			
19	$200-250$	$25-50$	—
20	$200-250$	>50	—
21	$250-300$	$25-50$	—
22	$250-300$	$50-75$	—
23	$250-300$	>75	—
24	$300-350$	$25-50$	—
25	$300-350$	$50-75$	—
26	$300-350$	>75	—
27	>350	$25-75$	—
28	>350	$75-100$	—
29	>350	>100	—
Displaced SRs			
SR bin	$p_{\mathrm{T}}^{\tau_{\mathrm{h}}2}$ [GeV]		
30	<110		
31	>110		

sample of same-charge $\tau_{\mathrm{h}}\tau_{\mathrm{h}}$ events. The fraction is found to be ≈10–15%, and depends on the p_{T} and decay mode of the τ_{h} candidate, as well as additional activity in an event from the presence of pileup. We parameterize the measurement in the τ_{h} p_{T} and decay mode, as well as the number of reconstructed primary vertices, to take these effects into account. The misidentification rate also depends on the jet flavor, i.e., whether the misidentified jet originates from the hadronization of light-flavor quarks, heavy-flavor quarks, or gluons, which cannot be reliably

determined in data. We assign a systematic uncertainty of 30% based on studies performed with simulation samples to account for the flavor dependence of the misidentification rate. The contribution of genuine τ_h candidates in the sideband regions selected with the relaxed identification requirement is taken into account when determining the background prediction as described in Ref. [37].

5.2 Estimation of backgrounds with two genuine τ_h

The background contribution with two genuine τ_h originates mainly from the $Z/\gamma* \to \tau\tau$ process. We estimate this background by means of "embedded" samples as described earlier. This method [41] generates a set of hybrid events that only rely on simulation for the τ lepton decays. Consequently, they provide a better description of the underlying event, pileup, additional jets, detector noise and resolution effects compared to the MC simulation.

We use a set of embedded samples in which both τ leptons are required to decay hadronically. We use an opposite-charge di-τ_h region in data to derive residual scale factors for the normalization of the embedded sample after all other correction factors are applied. This region consists of events passing the baseline selection, with the following additional requirements imposed on the mass and p_T of the di-τ_h system in order to improve the purity of genuine τ_h: $m_{\tau_h\tau_h} > 50\,\text{GeV}$, $p_T^{\tau_h\tau_h} > 50\,\text{GeV}$. In order to ensure orthogonality with the SRs and to suppress signal contamination, we require that events in this region must have $m_{T2} < 25\,\text{GeV}$ or $\Sigma m_T < 200\,\text{GeV}$. The contribution from $Z/\gamma* \to \tau\tau$ in this control region is enhanced by requiring $m_{\tau_h\tau_h} < 90\,\text{GeV}$. After subtracting the estimated contributions from misidentified τ_h events in this sample, we measure scale factors of 1.24 ± 0.03, 1.21 ± 0.03, and 1.16 ± 0.02 for 2016, 2017, and 2018 data, respectively, for the embedded events. We apply these scale factors, along with an uncertainty corresponding to the full size of their deviations from unity, to the normalization of the embedded sample.

The genuine τ_h background prediction from the embedded sample accounts for SM events originating from processes in which the branching fractions for di-τ and di-muon decays are identical, i.e., $Z/\gamma* \to \tau\tau$, $t\bar{t}$ (with or without extra vector bosons), single top quark, and diboson processes. Small contributions from top quark events in which the W boson from the top quark decay does not decay directly into a muon and a neutrino, e.g. from $W \to \tau\nu_\tau$, may arise in the sample selected to undergo the embedding process, resulting in a possible overestimation of the fraction of top quark events. In order to account for this effect, we check the normalization of top quark events estimated from the embedded sample in a control region selected by requiring at least one b-tagged jet, $m_{\tau_h\tau_h} > 100\,\text{GeV}$, and $p_T^{\text{miss}} > 50\,\text{GeV}$ in order to enrich the proportion of top quark events. Based on the level of agreement observed between data and the prediction from the embedded sample in this region, we assign an uncertainty of 10% to the expected fraction of top quark events in the embedded sample as estimated from simulation.

The embedded sample does not account for contributions from SM Higgs boson events, for which the di-τ and di-muon branching fractions are very different. We therefore include the estimated contribution from SM $H \to \tau\tau$ events from simulation in the total estimate of the genuine τ_h background. We find that the background contribution from SM $H \to \tau\tau$ events is negligible compared to the other backgrounds.

6 Systematic uncertainties

The dominant uncertainties in the background estimates are the statistical uncertainty driven by the limited event counts in the data sidebands or embedded samples used to obtain the estimates, and the systematic uncertainty (30%) assigned to the estimate of the τ_h misidentification rate that covers its dependence on jet flavor.

Because we use hybrid embedded events to estimate the background with two genuine τ_h, fewer uncertainties arise than in the case of wholly simulated samples. For this background, we propagate uncertainties related to the trigger efficiency, τ_h identification efficiency, and τ_h energy scale. An uncertainty of 10% is assigned to the expected fraction of top quark events in the embedded samples estimated from simulation, in order to account for any contamination from top quark events that do not contain muons originating directly from W boson decays in the events selected for embedding. We also assign a normalization uncertainty corresponding to the full size of the deviations from unity of the normalization scale factors derived from the $Z/\gamma* \to \tau\tau$ control region, weighted over the three years by the integrated luminosity of the data collected in each relative to the total. A 20% normalization uncertainty is assigned to the small contribution from SM $H \to \tau\tau$ events.

For the signal prediction obtained from simulation, we propagate experimental uncertainties for the trigger efficiency, τ_h identification efficiency, τ_h energy scale, b tagging efficiency, pileup reweighting, jet energy scale and resolution, and unclustered energy. We also take into account the uncertainty in the integrated luminosity measurement, which is 1.8% for the combined 2016–2018 data-taking period, with an improvement in precision relative to Refs. [66–68] reflecting the (uncorrelated) time evolution of some systematic effects. Uncertainties related to the renormalization and factorization scales, and to the modeling of ISR, are propagated to the signal prediction as well. Since the τ_h identification and trigger efficiency correction factors applied to simulation, which are obtained from samples of $Z/\gamma* \to \tau\tau$ events with promptly produced τ leptons, do not account for the dependence of the τ_h selection on the displacement of the decay position, we assign an additional uncertainty for this effect in signal events. The uncertainty is assessed via a comparison of τ_h impact parameter distributions between data and simulation in a control region that is mainly populated by $Z/\gamma* \to \tau\tau$ events, and the expected displacement of signal events for different $\widetilde{\tau}$ lifetimes. In order to probe the tails of the τ_h impact parameter distributions, which we expect to be populated by signal events with significant displacement, the data-to-simulation ratios observed in the control region at lower values of τ_h dxy significance and IP3D are extrapolated to higher values via a linear fit when deriving this uncertainty. The size of the uncertainty ranges from 3% for promptly decaying $\widetilde{\tau}$, to 45% for $\widetilde{\tau}$ with $c\tau_0 = 2.5\,\text{mm}$.

We treat statistical uncertainties as uncorrelated, while systematic uncertainties related to the same modeling effect are taken to be correlated across processes. Table 2 lists the ranges of uncertainty in the predicted yields for signal and background across all SRs corresponding to different sources.

7 Results and interpretation

Observed and predicted event yields for each SR, prior to the maximum likelihood fit to the data, are shown in Fig. 2 (upper) and summarized in Table 3 for the combination of the 2016, 2017, and 2018 datasets corresponding to a total integrated luminosity of $137\,\text{fb}^{-1}$. Figure 2 (lower) shows the background predictions after the maximum likelihood fit to the data under the background-only hypothesis. The data are consistent with the prediction for SM back-

Table 2: Uncertainties in the analysis affecting signal and the SM backgrounds. The ranges shown for signal correpond to a representative benchmark model of left-handed $\widetilde{\tau}$ pair production with m($\widetilde{\tau}_{\mathrm{L}}$)=150 GeV, m($\widetilde{\chi}_1^0$)=1 GeV.

	Uncertainty [%]		
Source	Genuine τ_{h}	Misidentified τ_{h}	Signal
Statistical	8.3–141	5.0–100	6.3–52
τ_{h} ID efficiency	7.2–7.8	—	6.2–6.4
τ_{h} ID vs displacement	—	—	3.0
τ_{h} trigger efficiency	3.1–4.2	—	6.9–14
τ_{h} energy scale	0.1–35	—	1.6–44
τ_{h} misidentification rate	—	30–56	—
$p_{\mathrm{T}}^{\mathrm{miss}}$ trigger efficiency	1.0	—	1.5
Embedded normalization	19	—	—
Embedded top quark fraction	1.0–3.8	—	—
Jet energy scale	—	—	0.7–32
Jet energy resolution	—	—	1.3–55
Unclustered energy	—	—	0.5–32
B–tagging	—	—	0.2–1.1
Pileup	—	—	1.0–28
Pre-fire	—	—	0.1–0.4
Integrated luminosity	—	—	1.8
ISR	—	—	0.1–16
Renormalization/factorization scale	—	—	0.4–3.6

ground.

We use these results to set upper limits on the cross section for the production of $\widetilde{\tau}$ pairs in the context of simplified models [26–28, 69] using all of the 31 exclusive SRs in a full statistical combination. The 95% CL upper limits on SUSY production cross sections are calculated using a modified frequentist approach with the $\mathrm{CL_s}$ criterion [70, 71]. An asymptotic approximation is used for the test statistic [72, 73]. The observed and predicted event yields in the SRs are used in the limit calculation, with uncertainties in the signal and background estimates included as nuisance parameters. The normalization uncertainties affecting background and signal predictions are generally assumed to be log-normally distributed. For statistical uncertainties limited by small event counts in the embedded or simulation samples, or in the sideband regions in the data used to estimate the misidentified τ_{h} background, we use a Poisson distribution. The nuisance parameters are allowed to vary within their uncertainties in the fit.

Expected and observed 95% CL cross section upper limits are shown in Fig. 3 for $\widetilde{\tau}$ pair production with promptly decaying $\widetilde{\tau}$s in the degenerate scenario, in which we assume that both left- and right-handed $\widetilde{\tau}$s are produced with the same mass, and in Fig. 4-5 in the purely left-handed and right-handed scenarios, respectively. In general, the cross section limits become less stringent for higher values of the $\widetilde{\chi}_1^0$ mass, due to the smaller experimental acceptance, caused in particular by the decreasing probability of the τ_{h} to exceed the 40 GeV $p_{\mathrm{T}}^{\tau_{\mathrm{h}}}$ threshold. Exclusion limits in the $\widetilde{\tau}$ vs $\widetilde{\chi}_1^0$ mass plane are presented in Fig. 6 for promptly decaying $\widetilde{\tau}$s in the degenerate and purely left-handed scenarios. Exclusion limits for the purely right-handed scenario are not shown, because our sensitivity in this scenario is not yet sufficient to exclude a sizeable region in the $\widetilde{\tau}$ vs $\widetilde{\chi}_1^0$ mass plane. Expected and observed 95% CL cross section upper limits are shown in Fig. 7 for long-lived $\widetilde{\tau}$s in the maximally-mixed scenario, under the hypothesis of a nearly massless LSP.

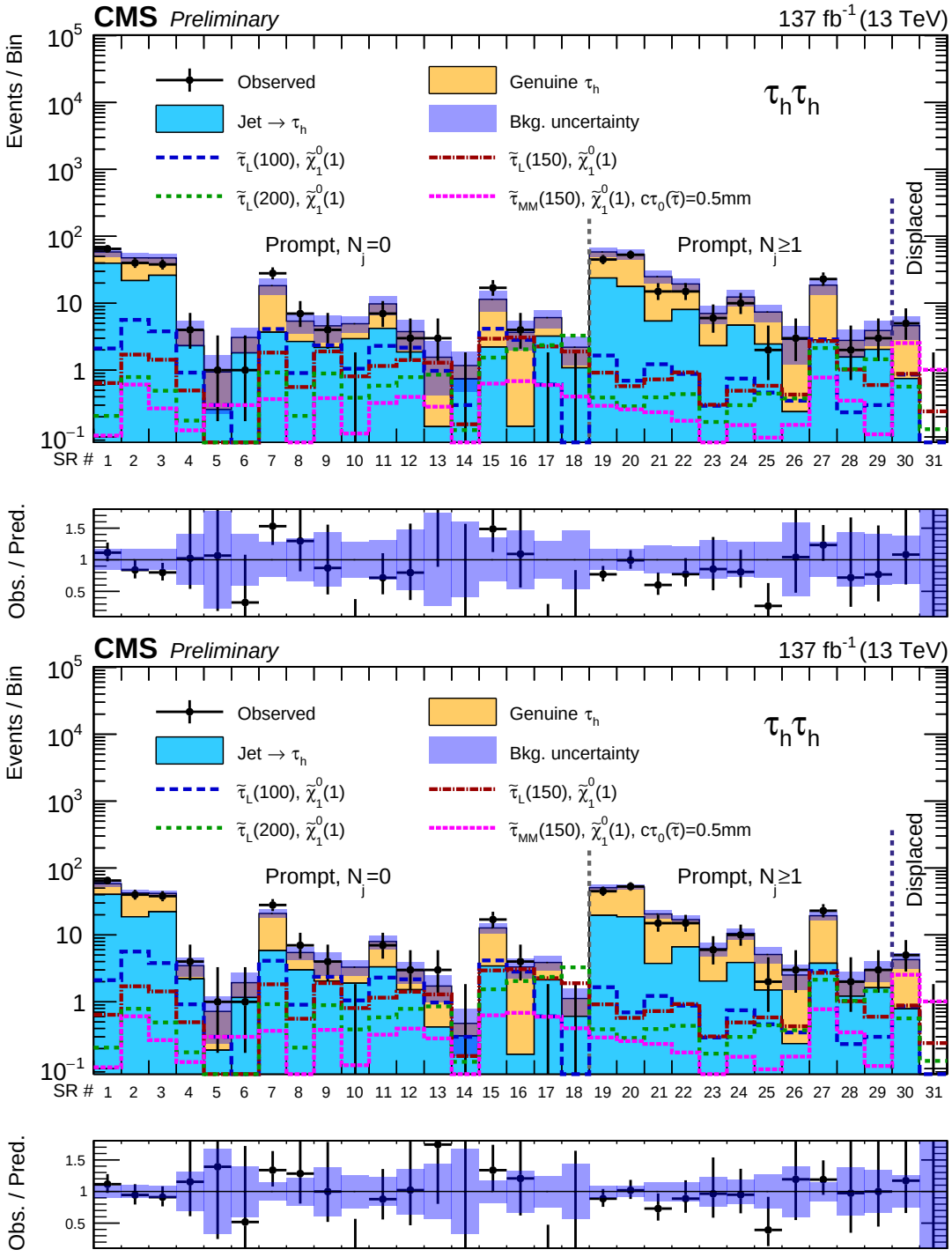

Figure 2: Event counts and predicted yields in each SR for the SM background before (upper) and after (lower) a maximum-likelihood fit to the data. The yields expected for 3 benchmark models of left-handed $\tilde{\tau}$ pair production assuming prompt $\tilde{\tau}$ decays, and one model of long-lived $\tilde{\tau}$ pair production in the maximally-mixed scenario are overlaid. The numbers in parentheses correspond to the masses of the $\tilde{\tau}$ and LSP in units of GeV for the different signal models. The first 29 bins correspond to the prompt SRs, while bins 30 and 31 correspond to the displaced SRs, as labelled in Table 1.

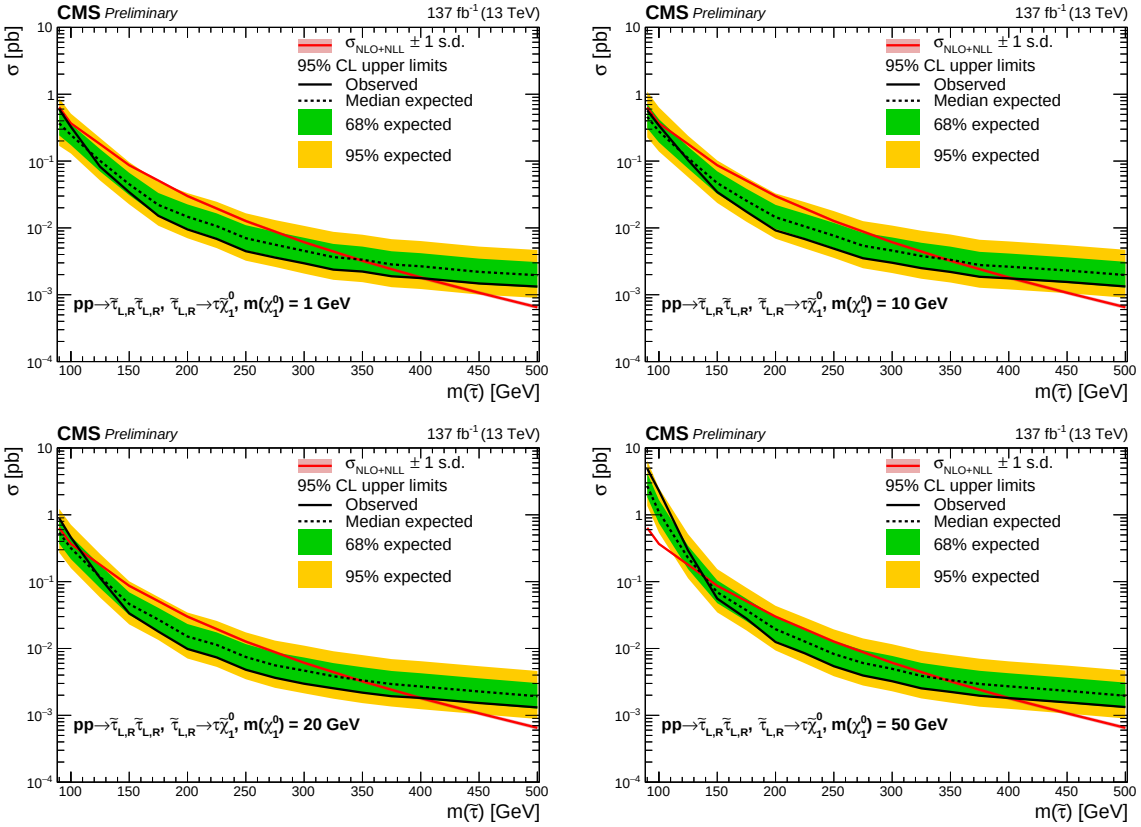

Figure 3: Expected and observed 95% CL cross section upper limits for the combined 2016, 2017, and 2018 datasets as a function of $\widetilde{\tau}$ mass in the degenerate $\widetilde{\tau}$ scenario for $\widetilde{\chi}_1^0$ masses of 1, 10, 20, and 50 GeV (upper left to lower right).

8 Summary

A search for direct τ slepton ($\widetilde{\tau}$) pair production has been performed in proton-proton collisions at a center-of-mass energy of 13 TeV in events with a τ lepton pair and significant missing transverse momentum. Both prompt and displaced decays of the τ slepton are studied. Thirty-one different search regions are used in the analysis, based on kinematic observables that exploit expected differences between signal and background. The data used for this search correspond to an integrated luminosity of 137 fb^{-1} collected in 2016, 2017, and 2018 with the CMS detector. No excess of events above the expected standard model background has been observed. Upper limits have been set on the cross section for direct $\widetilde{\tau}$ pair production for simplified models in which each $\widetilde{\tau}$ decays to a τ lepton and the lightest neutralino, with the latter being assumed to be the lightest supersymmetric particle (LSP). For purely left-handed $\widetilde{\tau}$ pair production with prompt decays, $\widetilde{\tau}$ masses between 115 and 340 GeV are excluded for the case of a nearly massless LSP. In scenarios with macroscopic $\widetilde{\tau}$ decay lengths corresponding to $c\tau_0$ =0.1 mm, masses between 150 and 220 GeV are excluded for the case that the LSP is nearly massless.

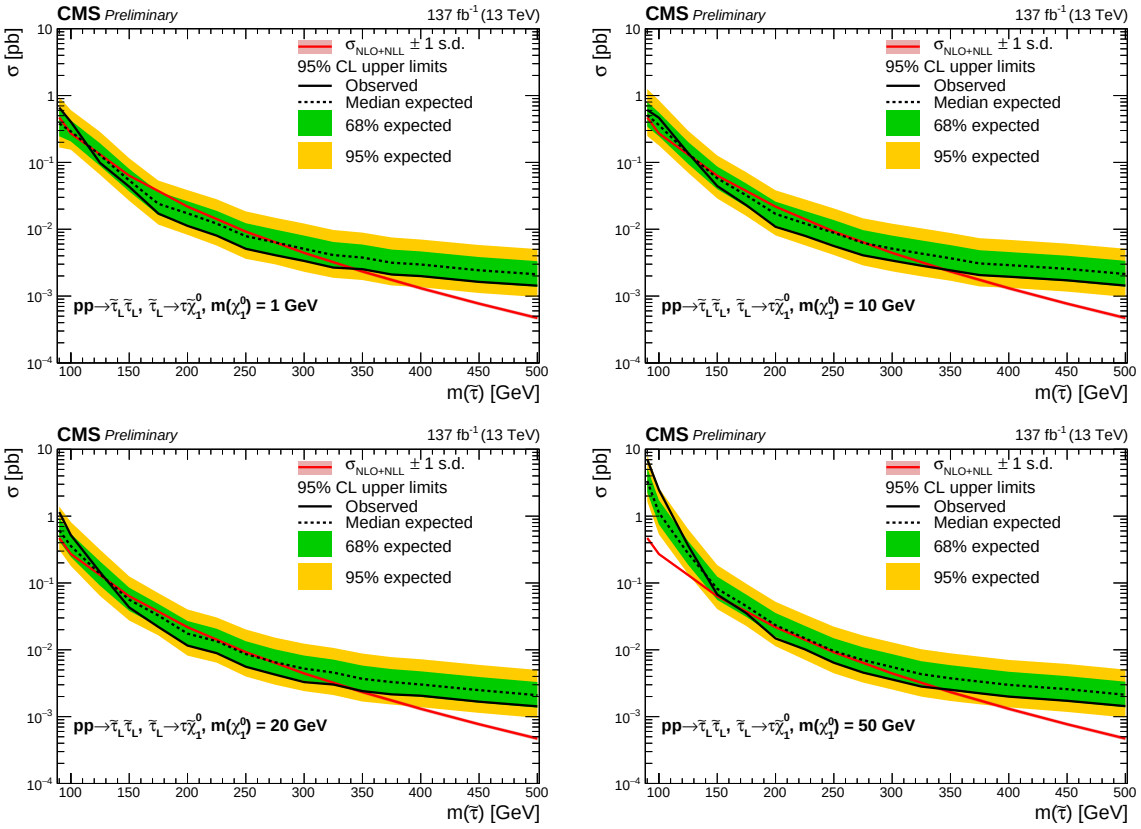

Figure 4: Expected and observed 95% CL cross section upper limits for the combined 2016, 2017, and 2018 datasets as a function of $\widetilde{\tau}$ mass in the purely left-handed $\widetilde{\tau}$ scenario for $\widetilde{\chi}_1^0$ masses of 1, 10, 20, and 50 GeV (upper left to lower right).

Table 3: Predicted SM background yields, observed event counts, and predicted signal yields for two benchmark models with a $\widetilde{\tau}$ mass of 150 GeV and an LSP mass of 1 GeV, in all prompt and displaced SRs as labelled in Table 1, corresponding to 137 fb^{-1} of data. For the prompt signal model shown, we assume left-handed $\widetilde{\tau}$ pair production, while for the displaced signal model we assume a maximally-mixed scenario and $c\tau_0(\widetilde{\tau}) = 0.5$ mm. The uncertainties listed are the sum in quadrature of statistical and systematic uncertainties. For any estimate with no events in the data sideband, embedded, or simulation sample corresponding to a given SR selection, we provide the one standard deviation upper bound evaluated for that estimate.

SR bin	Genuine τ_h	Misidentified τ_h	Total SM	Observed	Prompt signal	Displaced τ_h signal
1	18.81 ± 4.37	39.58 ± 8.53	58.38 ± 9.59	65	0.64 ± 0.15	0.10 ± 0.06
2	25.90 ± 6.16	21.78 ± 5.48	47.68 ± 8.25	40	1.71 ± 0.32	0.60 ± 0.20
3	21.39 ± 4.85	26.12 ± 6.02	47.51 ± 7.73	38	1.43 ± 0.28	0.27 ± 0.11
4	$1.30^{+0.96}_{-0.62}$	$2.11^{+1.55}_{-1.35}$	$3.41^{+1.82}_{-1.49}$	4	0.50 ± 0.13	0.13 ± 0.07
5	$0.54^{+0.48}_{-0.34}$	$0.09^{+0.74}_{-0.09}$	$0.64^{+0.88}_{-0.36}$	1	0.05 ± 0.03	< 0.55
6	$0.95^{+0.94}_{-0.55}$	$1.58^{+1.14}_{-0.91}$	$2.53^{+1.48}_{-1.06}$	1	0.02 ± 0.02	< 0.55
7	14.61 ± 3.85	3.68 ± 3.01	18.29 ± 4.89	28	1.83 ± 0.32	0.37 ± 0.16
8	$2.49^{+1.09}_{-0.86}$	2.68 ± 1.54	$5.16^{+1.88}_{-1.76}$	7	0.56 ± 0.13	0.06 ± 0.05
9	$2.11^{+1.26}_{-0.95}$	2.18 ± 1.63	$4.29^{+2.06}_{-1.88}$	4	1.91 ± 0.34	0.38 ± 0.13
10	$1.77^{+0.92}_{-0.67}$	$2.73^{+1.27}_{-1.07}$	$4.50^{+1.56}_{-1.26}$	0	0.81 ± 0.17	0.11 ± 0.05
11	$5.21^{+2.13}_{-1.80}$	4.20 ± 2.24	$9.41^{+3.09}_{-2.87}$	7	1.16 ± 0.21	0.32 ± 0.12
12	$1.52^{+1.31}_{-0.90}$	$1.67^{+1.44}_{-1.17}$	$3.19^{+1.94}_{-1.47}$	3	1.42 ± 0.26	0.39 ± 0.14
13	$1.06^{+1.05}_{-0.62}$	$0.07^{+1.03}_{-0.07}$	$1.14^{+1.47}_{-0.62}$	3	1.29 ± 0.24	0.28 ± 0.12
14	$0.22^{+0.50}_{-0.18}$	$0.48^{+0.78}_{-0.42}$	$0.70^{+0.93}_{-0.46}$	0	0.15 ± 0.06	0.02 ± 0.03
15	$8.86^{+2.87}_{-2.58}$	2.21 ± 2.63	$11.07^{+3.89}_{-3.68}$	17	2.95 ± 0.41	0.62 ± 0.20
16	$3.17^{+1.64}_{-1.30}$	< 1.05	$3.17^{+1.95}_{-1.30}$	4	3.08 ± 0.48	0.68 ± 0.21
17	$2.51^{+1.45}_{-1.06}$	$3.00^{+1.48}_{-1.28}$	$5.51^{+2.07}_{-1.66}$	0	2.26 ± 0.35	0.60 ± 0.19
18	$0.74^{+0.99}_{-0.51}$	$0.87^{+0.80}_{-0.55}$	$1.62^{+1.28}_{-0.75}$	0	1.90 ± 0.32	0.40 ± 0.14
19	34.60 ± 7.87	23.80 ± 5.50	58.40 ± 9.61	45	0.93 ± 0.19	0.30 ± 0.12
20	35.70 ± 7.65	17.74 ± 4.78	53.44 ± 9.02	53	0.58 ± 0.13	0.26 ± 0.10
21	19.51 ± 4.89	5.41 ± 2.56	24.92 ± 5.52	15	0.74 ± 0.16	0.24 ± 0.11
22	11.37 ± 2.98	8.03 ± 2.96	19.40 ± 4.20	15	0.94 ± 0.19	0.17 ± 0.09
23	$4.51^{+1.51}_{-1.33}$	2.31 ± 1.60	$6.82^{+2.20}_{-2.08}$	6	0.31 ± 0.09	0.02 ± 0.02
24	$7.31^{+2.66}_{-2.36}$	4.69 ± 2.41	$12.00^{+3.59}_{-3.38}$	10	0.50 ± 0.13	0.15 ± 0.07
25	$4.60^{+1.86}_{-1.56}$	$2.26^{+1.37}_{-1.21}$	$6.87^{+2.31}_{-1.97}$	2	0.59 ± 0.14	0.10 ± 0.05
26	$2.31^{+1.34}_{-0.99}$	< 1.31	$2.31^{+1.88}_{-0.99}$	3	0.44 ± 0.10	0.15 ± 0.07
27	15.80 ± 4.11	2.84 ± 3.11	18.64 ± 5.15	23	2.77 ± 0.42	0.78 ± 0.23
28	$0.91^{+0.90}_{-0.53}$	$1.42^{+1.15}_{-0.90}$	$2.33^{+1.46}_{-1.05}$	2	1.04 ± 0.20	0.35 ± 0.12
29	$1.49^{+1.21}_{-0.78}$	$1.91^{+1.40}_{-1.14}$	$3.40^{+1.85}_{-1.38}$	3	0.61 ± 0.13	0.11 ± 0.05
30	$3.58^{+1.55}_{-1.26}$	$0.69^{+1.28}_{-0.69}$	$4.27^{+2.01}_{-1.45}$	5	0.89 ± 0.16	2.54 ± 0.69
31	< 0.55	< 0.37	$0.00^{+0.66}_{-0.00}$	0	0.24 ± 0.07	1.01 ± 0.30

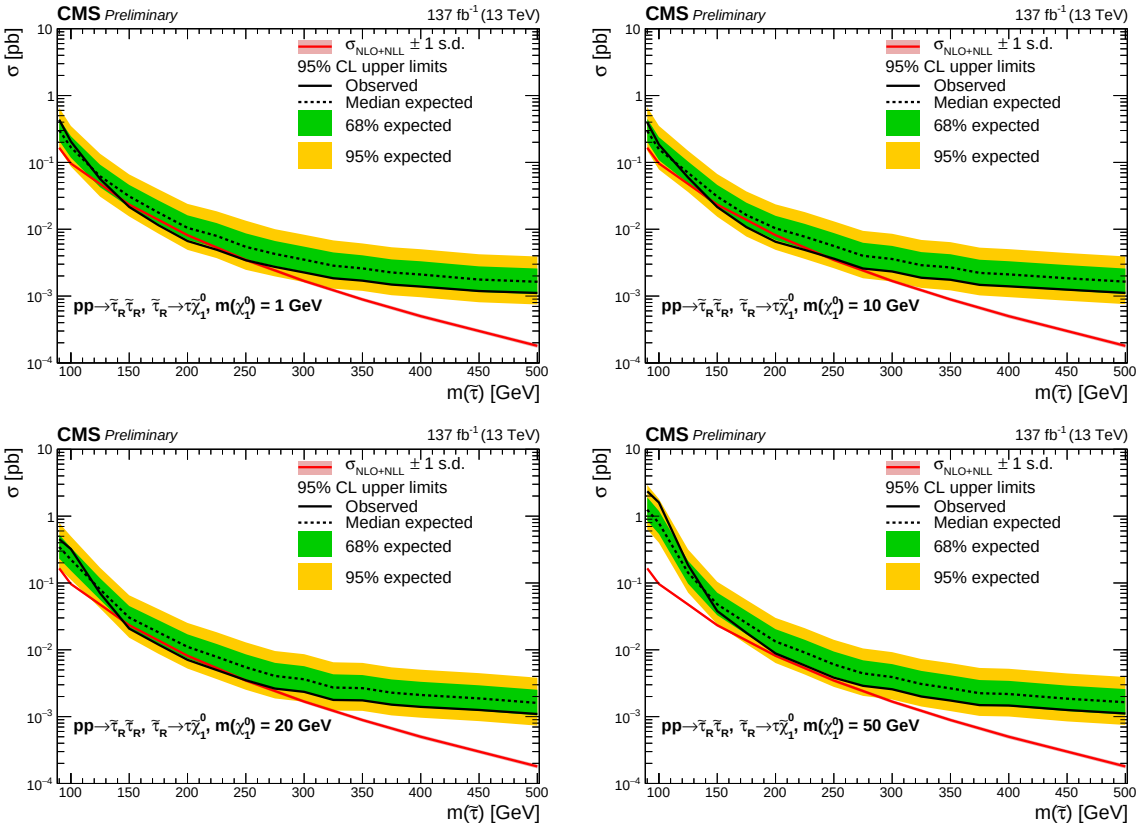

Figure 5: Expected and observed 95% CL cross section upper limits for the combined 2016, 2017, and 2018 datasets as a function of $\tilde{\tau}$ mass in the purely right-handed $\tilde{\tau}$ scenario for $\tilde{\chi}_1^0$ masses of 1, 10, 20, and 50 GeV (upper left to lower right).

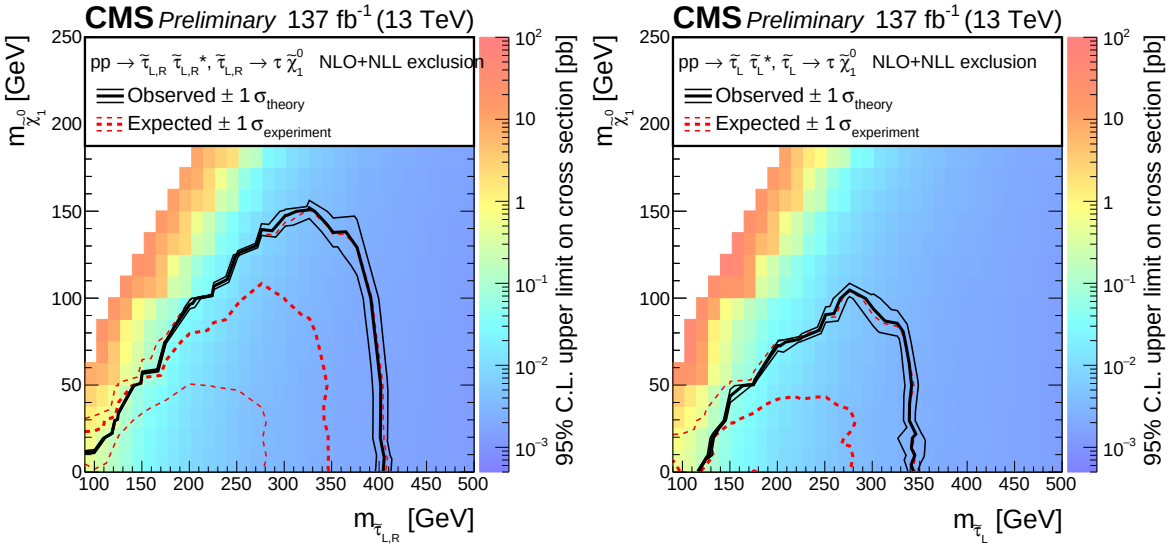

Figure 6: Upper limits at 95% CL on the cross section for degenerate (left) and purely left-handed (right) $\widetilde{\tau}$ pair production in the $m(\widetilde{\tau}) - m(\widetilde{\chi}_1^0)$ plane for the combined 2016, 2017, and 2018 datasets. The thick black (red) curves show the observed (expected) exclusion limits assuming NLO+NLL predictions for the signal cross sections. The thin black curves represent the variations in the observed limits obtained when varying the cross sections by their ± 1 standard deviation uncertainties. The thin dashed red curves indicate the region containing 68% of the distribution of limits expected under the background-only hypothesis.

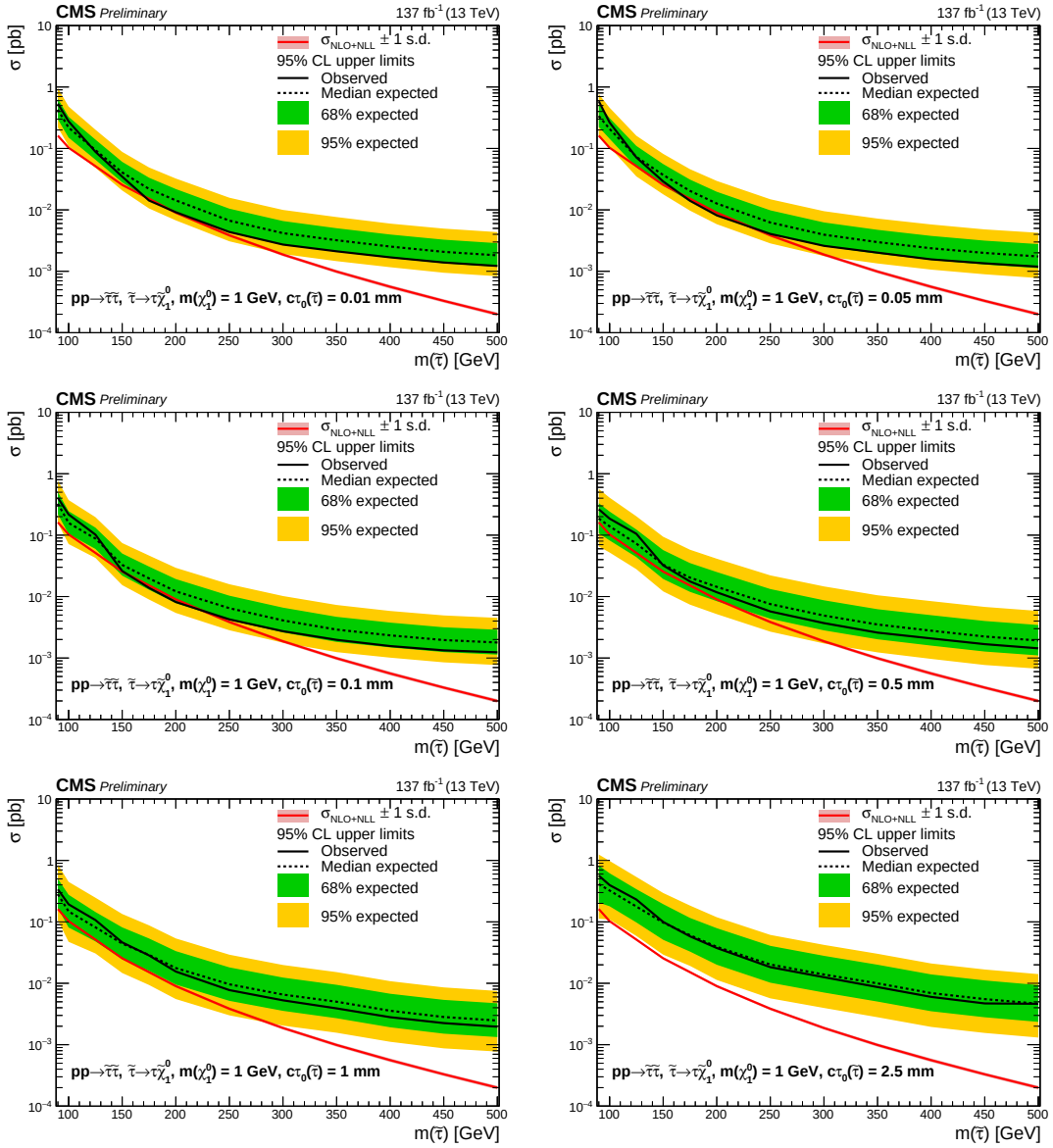

Figure 7: Expected and observed 95% CL cross section upper limits for the combined 2016, 2017, and 2018 datasets as a function of $\tilde{\tau}$ mass for long-lived $\tilde{\tau}$ in the maximally-mixed scenario for an LSP mass of 1 GeV, and for $c\tau_0$ values of 0.01, 0.05, 0.1, 0.5, 1, and 2.5 mm (upper left to lower right).

References

[1] P. Ramond, "Dual theory for free fermions", *Phys. Rev. D* **3** (1971) 2415, doi:10.1103/PhysRevD.3.2415.

[2] Y. A. Gol'fand and E. P. Likhtman, "Extension of the algebra of Poincaré group generators and violation of P invariance", *JETP Lett.* **13** (1971) 323.

[3] A. Neveu and J. H. Schwarz, "Factorizable dual model of pions", *Nucl. Phys. B* **31** (1971) 86, doi:10.1016/0550-3213(71)90448-2.

[4] D. V. Volkov and V. P. Akulov, "Possible universal neutrino interaction", *JETP Lett.* **16** (1972) 438.

[5] J. Wess and B. Zumino, "A Lagrangian model invariant under supergauge transformations", *Phys. Lett. B* **49** (1974) 52, doi:10.1016/0370-2693(74)90578-4.

[6] J. Wess and B. Zumino, "Supergauge transformations in four dimensions", *Nucl. Phys. B* **70** (1974) 39, doi:10.1016/0550-3213(74)90355-1.

[7] P. Fayet, "Supergauge invariant extension of the Higgs mechanism and a model for the electron and its neutrino", *Nucl. Phys. B* **90** (1975) 104, doi:10.1016/0550-3213(75)90636-7.

[8] H. P. Nilles, "Supersymmetry, supergravity and particle physics", *Phys. Rep.* **110** (1984) 1, doi:10.1016/0370-1573(84)90008-5.

[9] E. Gildener, "Gauge Symmetry Hierarchies", *Phys. Rev. D* **14** (1976) 1667, doi:10.1103/PhysRevD.14.1667.

[10] M. J. G. Veltman, "Second Threshold in Weak Interactions", *Acta Phys. Polon. B* **8** (1977) 475.

[11] G. 't Hooft, "Naturalness, chiral symmetry, and spontaneous chiral symmetry breaking", *NATO Sci. Ser. B* **59** (1980) 135.

[12] E. Witten, "Dynamical breaking of supersymmetry", *Nucl. Phys. B* **188** (1981) 513, doi:10.1016/0550-3213(81)90006-7.

[13] G. R. Farrar and P. Fayet, "Phenomenology of the production, decay, and detection of new hadronic states associated with supersymmetry", *Phys. Lett. B* **76** (1978) 575, doi:10.1016/0370-2693(78)90858-4.

[14] H. Goldberg, "Constraint on the Photino Mass from Cosmology", *Phys. Rev. Lett.* **50** (1983) 1419, doi:10.1103/PhysRevLett.50.1419. [Erratum: Phys. Rev. Lett.103,099905(2009)].

[15] J. R. Ellis et al., "Supersymmetric Relics from the Big Bang", *Nucl. Phys. B* **238** (1984) 453–476, doi:10.1016/0550-3213(84)90461-9.

[16] G. Jungman, M. Kamionkowski, and K. Griest, "Supersymmetric dark matter", *Phys. Rept.* **267** (1996) 195, doi:10.1016/0370-1573(95)00058-5, arXiv:hep-ph/9506380.

[17] G. Hinshaw et al., "Nine-year Wilkinson Microwave Anisotropy Probe (WMAP) observations: cosmological parameter results", *Astrophys. J. Suppl.* **208** (2013) 19, doi:10.1088/0067-0049/208/2/19, arXiv:1212.5226.

[18] K. Griest and D. Seckel, "Three exceptions in the calculation of relic abundances", *Phys. Rev. D* **43** (1991) 3191, doi:10.1103/PhysRevD.43.3191.

[19] D. A. Vasquez, G. Bélanger, and C. Boehm, "Revisiting light neutralino scenarios in the MSSM", *Phys. Rev. D* **84** (2011) 095015, doi:10.1103/PhysRevD.84.095015, arXiv:1108.1338.

[20] S. F. King, J. P. Roberts, and D. P. Roy, "Natural dark matter in SUSY GUTs with non-universal gaugino masses", *JHEP* **10** (2007) 106, doi:10.1088/1126-6708/2007/10/106, arXiv:0705.4219.

[21] M. Battaglia et al., "Proposed post-LEP benchmarks for supersymmetry", *Eur. Phys. J. C* **22** (2001) 535, doi:10.1007/s100520100792, arXiv:hep-ph/0106204.

[22] R. L. Arnowitt et al., "Determining the dark matter relic density in the minimal supergravity stau-neutralino coannihilation region at the Large Hadron Collider", *Phys. Rev. Lett.* **100** (2008) 231802, doi:10.1103/PhysRevLett.100.231802, arXiv:0802.2968.

[23] G. Bélanger, S. Biswas, C. Boehm, and B. Mukhopadhyaya, "Light neutralino dark matter in the MSSM and its implication for LHC searches for staus", *JHEP* **12** (2012) 076, doi:10.1007/JHEP12(2012)076, arXiv:1206.5404.

[24] E. Arganda, V. Martin-Lozano, A. D. Medina, and N. Mileo, "Potential discovery of staus through heavy Higgs boson decays at the LHC", *JHEP* **09** (2018) 056, doi:10.1007/JHEP09(2018)056, arXiv:1804.10698.

[25] J. A. Evans and J. Shelton, "Long-Lived Staus and Displaced Leptons at the LHC", *JHEP* **04** (2016) 056, doi:10.1007/JHEP04(2016)056, arXiv:1601.01326.

[26] J. Alwall, P. Schuster, and N. Toro, "Simplified models for a first characterization of new physics at the LHC", *Phys. Rev. D* **79** (2009) 075020, doi:10.1103/PhysRevD.79.075020, arXiv:0810.3921.

[27] J. Alwall, M.-P. Le, M. Lisanti, and J. Wacker, "Model-independent jets plus missing energy searches", *Phys. Rev. D* **79** (2009) 015005, doi:10.1103/PhysRevD.79.015005, arXiv:0809.3264.

[28] LHC New Physics Working Group, "Simplified models for LHC new physics searches", *J. Phys. G* **39** (2012) 105005, doi:10.1088/0954-3899/39/10/105005, arXiv:1105.2838.

[29] ALEPH Collaboration, "Search for scalar leptons in e^+e^- collisions at center-of-mass energies up to 209 GeV", *Phys. Lett. B* **526** (2002) 206, doi:10.1016/S0370-2693(01)01494-0, arXiv:hep-ex/0112011.

[30] DELPHI Collaboration, "Searches for supersymmetric particles in e^+e^- collisions up to 208 GeV and interpretation of the results within the MSSM", *Eur. Phys. J. C* **31** (2003) 421, doi:10.1140/epjc/s2003-01355-5, arXiv:hep-ex/0311019.

[31] L3 Collaboration, "Search for scalar leptons and scalar quarks at LEP", *Phys. Lett. B* **580** (2004) 37, doi:10.1016/j.physletb.2003.10.010, arXiv:hep-ex/0310007.

[32] OPAL Collaboration, "Search for anomalous production of dilepton events with missing transverse momentum in e^+e^- collisions at $\sqrt{s}$ = 183 GeV to 209 GeV", *Eur. Phys. J. C* **32** (2004) 453, doi:10.1140/epjc/s2003-01466-y, arXiv:hep-ex/0309014.

[33] ATLAS Collaboration, "Search for the direct production of charginos, neutralinos and staus in final states with at least two hadronically decaying taus and missing transverse momentum in pp collisions at $\sqrt{s}$ = 8 TeV with the ATLAS detector", *JHEP* **10** (2014) 96, doi:10.1007/JHEP10(2014)096, arXiv:1407.0350.

[34] ATLAS Collaboration, "Search for the electroweak production of supersymmetric particles in $\sqrt{s} = 8$ TeV pp collisions with the ATLAS detector", *Phys. Rev. D* **93** (2016) 052002, doi:10.1103/PhysRevD.93.052002, arXiv:1509.07152.

[35] CMS Collaboration, "Search for electroweak production of charginos in final states with two tau leptons in pp collisions at $\sqrt{s} = 8$ TeV", *JHEP* **04** (2017) 018, doi:10.1007/JHEP04(2017)018, arXiv:1610.04870.

[36] ATLAS Collaboration, "Search for direct stau production in events with two hadronic τ-leptons in $\sqrt{s} = 13$ TeV pp collisions with the ATLAS detector", *Phys. Rev. D* **101** (2020) 032009, doi:10.1103/PhysRevD.101.032009, arXiv:1911.06660.

[37] CMS Collaboration, "Search for direct pair production of supersymmetric partners to the τ lepton in proton-proton collisions at $\sqrt{s} = 13$ TeV", *Eur. Phys. J. C* **80** (2020) 189, doi:10.1140/epjc/s10052-020-7739-7, arXiv:1907.13179.

[38] B. Fuks, M. Klasen, D. R. Lamprea, and M. Rothering, "Revisiting slepton pair production at the Large Hadron Collider", *JHEP* **01** (2014) 168, doi:10.1007/JHEP01(2014)168, arXiv:1310.2621.

[39] OPAL Collaboration, "Searches for gauge-mediated supersymmetry breaking topologies in e^+e^- collisions at LEP2", *Eur. Phys. J. C* **46** (2006) 307–341, doi:10.1140/epjc/s2006-02524-8, arXiv:hep-ex/0507048.

[40] ATLAS Collaboration, "Search for displaced leptons in $\sqrt{s} = 13$ TeV pp collisions with the ATLAS detector", 11, 2020. arXiv:2011.07812. Submitted to *Phys. Rev. Lett.*

[41] CMS Collaboration, "An embedding technique to determine $\tau\tau$ backgrounds in proton-proton collision data", *JINST* **14** (2019), no. 06, P06032, doi:10.1088/1748-0221/14/06/P06032, arXiv:1903.01216.

[42] CMS Collaboration, "The CMS trigger system", *JINST* **12** (2017) P01020, doi:10.1088/1748-0221/12/01/P01020, arXiv:1609.02366.

[43] CMS Collaboration, "The CMS experiment at the CERN LHC", *JINST* **3** (2008) S08004, doi:10.1088/1748-0221/3/08/S08004.

[44] CMS Collaboration, "Particle-flow reconstruction and global event description with the CMS detector", *JINST* **12** (2017) P10003, doi:10.1088/1748-0221/12/10/P10003, arXiv:1706.04965.

[45] CMS Collaboration, "Performance of missing transverse momentum reconstruction in proton-proton collisions at $\sqrt{s} = 13$ TeV using the CMS detector", *JINST* **14** (2019) P07004, doi:10.1088/1748-0221/14/07/P07004, arXiv:1903.06078.

[46] M. Cacciari, G. P. Salam, and G. Soyez, "The anti-k_T jet clustering algorithm", *JHEP* **04** (2008) 063, doi:10.1088/1126-6708/2008/04/063, arXiv:0802.1189.

[47] M. Cacciari, G. P. Salam, and G. Soyez, "FastJet user manual", *Eur. Phys. J. C* **72** (2012) 1896, doi:10.1140/epjc/s10052-012-1896-2, arXiv:1111.6097.

[48] CMS Collaboration, "Study of pileup removal algorithms for jets", CMS Physics Analysis Summary CMS-PAS-JME-14-001, 2014.

[49] CMS Collaboration, "Identification of heavy-flavour jets with the CMS detector in pp collisions at 13 TeV", *JINST* **13** (2018) P05011, doi:10.1088/1748-0221/13/05/P05011, arXiv:1712.07158.

[50] CMS Collaboration, "Performance of reconstruction and identification of τ leptons decaying to hadrons and ν_τ in pp collisions at $\sqrt{s} = 13$ TeV", *JINST* **13** (2018) P10005, doi:10.1088/1748-0221/13/10/P10005, arXiv:1809.02816.

[51] J. Alwall et al., "The automated computation of tree-level and next-to-leading order differential cross sections, and their matching to parton shower simulations", *JHEP* **07** (2014) 079, doi:10.1007/JHEP07(2014)079, arXiv:1405.0301.

[52] T. Sjöstrand et al., "An introduction to PYTHIA 8.2", *Comput. Phys. Commun.* **191** (2015) 159, doi:10.1016/j.cpc.2015.01.024, arXiv:1410.3012.

[53] CMS Collaboration, "Event generator tunes obtained from underlying event and multiparton scattering measurements", *Eur. Phys. J. C* **76** (2016) 155, doi:10.1140/epjc/s10052-016-3988-x, arXiv:1512.00815.

[54] CMS Collaboration, "Extraction and validation of a new set of CMS PYTHIA8 tunes from underlying-event measurements", *Eur. Phys. J. C* **80** (2020) 4, doi:10.1140/epjc/s10052-019-7499-4, arXiv:1903.12179.

[55] NNPDF Collaboration, "Parton distributions for the LHC Run II", *JHEP* **04** (2015) 040, doi:10.1007/JHEP04(2015)040, arXiv:1410.8849.

[56] GEANT4 Collaboration, "GEANT4 — a simulation toolkit", *Nucl. Instrum. Meth. A* **506** (2003) 250, doi:10.1016/S0168-9002(03)01368-8.

[57] A. Kalogeropoulos and J. Alwall, "The SysCalc code: A tool to derive theoretical systematic uncertainties", 2018. arXiv:1801.08401.

[58] P. Nason, "A new method for combining NLO QCD with shower Monte Carlo algorithms", *JHEP* **11** (2004) 040, doi:10.1088/1126-6708/2004/11/040, arXiv:hep-ph/0409146.

[59] S. Frixione, P. Nason, and C. Oleari, "Matching NLO QCD computations with parton shower simulations: the POWHEG method", *JHEP* **11** (2007) 070, doi:10.1088/1126-6708/2007/11/070, arXiv:0709.2092.

[60] S. Alioli, P. Nason, C. Oleari, and E. Re, "A general framework for implementing NLO calculations in shower Monte Carlo programs: the POWHEG BOX", *JHEP* **06** (2010) 043, doi:10.1007/JHEP06(2010)043, arXiv:1002.2581.

[61] E. Re, "Single-top Wt-channel production matched with parton showers using the POWHEG method", *Eur. Phys. J. C* **71** (2011) 1547, doi:10.1140/epjc/s10052-011-1547-z, arXiv:1009.2450.

[62] CMS Collaboration, "Search for top-squark pair production in the single-lepton final state in pp collisions at $\sqrt{s}$ = 8 TeV", *Eur. Phys. J. C* **73** (2013) 2677, doi:10.1140/epjc/s10052-013-2677-2, arXiv:1308.1586.

[63] C. G. Lester and D. J. Summers, "Measuring masses of semi-invisibly decaying particle pairs produced at hadron colliders", *Phys. Lett. B* **463** (1999) 99, doi:10.1016/S0370-2693(99)00945-4, arXiv:hep-ph/9906349.

[64] A. Barr, C. Lester, and P. Stephens, "m_{T2}: the truth behind the glamour", *J. Phys. G* **29** (2003) 2343, doi:10.1088/0954-3899/29/10/304, arXiv:hep-ph/0304226.

[65] C. G. Lester and B. Nachman, "Bisection-based asymmetric m_{T2} computation: a higher precision calculator than existing symmetric methods", *JHEP* **03** (2015) 100, doi:10.1007/JHEP03(2015)100, arXiv:1411.4312.

[66] CMS Collaboration, "Precision luminosity measurement in proton-proton collisions at $\sqrt{s} = 13$ TeV in 2015 and 2016 at CMS", 2021. arXiv:2104.01927. Submitted to *Eur. Phys. J. C*.

[67] CMS Collaboration, "CMS luminosity measurement for the 2017 data-taking period at $\sqrt{s} = 13$ TeV", CMS Physics Analysis Summary CMS-PAS-LUM-17-004, 2018.

[68] CMS Collaboration, "CMS luminosity measurement for the 2018 data-taking period at $\sqrt{s} = 13$ TeV", CMS Physics Analysis Summary CMS-PAS-LUM-18-002, 2019.

[69] CMS Collaboration, "Interpretation of searches for supersymmetry with simplified models", *Phys. Rev. D* **88** (2013) 052017, doi:10.1103/PhysRevD.88.052017, arXiv:1301.2175.

[70] T. Junk, "Confidence level computation for combining searches with small statistics", *Nucl. Instrum. Meth. A* **434** (1999) 435, doi:10.1016/S0168-9002(99)00498-2, arXiv:hep-ex/9902006.

[71] A. L. Read, "Presentation of search results: the $\mathrm{CL_s}$ technique", *J. Phys. G* **28** (2002) 2693, doi:10.1088/0954-3899/28/10/313.

[72] The ATLAS Collaboration, The CMS Collaboration, The LHC Higgs Combination Group, "Procedure for the LHC Higgs boson search combination in Summer 2011", Technical Report CMS-NOTE-2011-005, ATL-PHYS-PUB-2011-11, 2011.

[73] G. Cowan, K. Cranmer, E. Gross, and O. Vitells, "Asymptotic formulae for likelihood-based tests of new physics", *Eur. Phys. J. C* **71** (2011) 1554, doi:10.1140/epjc/s10052-011-1554-0, arXiv:1007.1727. [Erratum: doi:10.1140/epjc/s10052-013-2501-z].